NASA TECHNICAL NOTE

NASA TN D-7748

NASA TN D-7748

AN ELASTOPLASTIC ANALYSIS OF A UNIAXIALLY LOADED SHEET WITH AN INTERFERENCE-FIT BOLT

by John H. Crews, Jr.

Langley Research Center

Hampton, Va. 23665

NATIONAL AERONAUTICS AND SPACE ADMINISTRATION • WASHINGTON, D. C. • OCTOBER 1974

AN ELASTOPLASTIC ANALYSIS OF A UNIAXIALLY LOADED SHEET WITH AN INTERFERENCE-FIT BOLT

By John H. Crews, Jr.
Langley Research Center

SUMMARY

The stresses and strains in a uniaxially loaded sheet with an unloaded interference-fit bolt were calculated by an elastoplastic finite-element analysis. The material properties represented a 7075-T6 aluminum-alloy sheet and a steel bolt. The analysis considered the two ideal cases of no slip and no friction at the bolt-sheet interface for a single combination of bolt diameter, interference level, and cyclic loading which might be typical of aircraft structures.

When the bolt was inserted, the sheet deformed plastically near the hole; the first tensile load cycle produced additional yielding, but subsequent cycles to the same level caused only elastic cyclic stresses. These stresses together with fatigue data for unnotched specimens were used to estimate crack initiation periods and initiation sites. The cases analyzed with interference-fit bolts were predicted to have crack initiation periods which were about 50 times that for a clearance-fit bolt. Crack initiation was predicted to occur on the transverse axis at a distance of about one radius from the hole. The crack initiation predictions agreed reasonably well with fatigue data from the literature.

INTRODUCTION

In recent years, interference-fit bolts have been commonly used to achieve long structural fatigue life. This long life can be explained by the effect of the interference-fit bolt on the stresses near the bolt hole. However, stress analyses to date have not adequately accounted for material yielding around the hole and, thus, cannot accurately predict the magnitude of the effect. For example, the analysis in reference 1 is limited to elastic behavior. The analysis in reference 2 applies only to elasto-perfectly-plastic materials. The analysis in reference 3 is for a strain-hardening sheet material. That analysis, however, is based on the assumption that the bolt is inserted and the sheet is loaded simultaneously; whereas, in practice the bolt would be inserted before the sheet is loaded. Because each action (bolt insertion and sheet loading) can cause the sheet to yield, they should be analyzed sequentially to account for the history dependence of plastic strains.

In the present study, elastoplastic stresses and strains were analyzed for a strain-hardening sheet material with due regard for the bolt insertion and sheet loading sequence. The material properties represented a 7075-T6 aluminum-alloy sheet and a steel bolt. The analysis is based upon the elastoplastic finite-element program described in reference 4. It considers the two ideal bolt-to-sheet interface conditions (a no-slip interface and a no-friction interface) which are expected to bracket the real interface condition of partial friction. The analysis was conducted for a single combination of bolt diameter, interference level, and cyclic loading which might be typical of aircraft structures.

The calculated stresses and strains, presented as local distributions near the bolt hole, are discussed; they are used, first, to determine the loads which separate the sheet from the bolt and, second, to estimate the fatigue life improvement when a clearance-fit bolt is replaced by an interference-fit bolt.

SYMBOLS

Although values are given in the SI Units in this report, some of the calculations were made in the U.S. Customary Units. Factors relating the two systems are given in reference 5.

E	Young's modulus, N/m^2
I	interference, difference between bolt and hole diameters, m
r,θ	polar coordinates, m and deg
R	radius of bolt hole, m
S	nominal gross-section stress, N/m^2
w	width of sheet, m
x,y	Cartesian coordinates, m
$\gamma_{r\theta}$	shear strain component in polar coordinates
ϵ	uniaxial normal strain
$\epsilon_{rr},\epsilon_{\theta\theta}$	normal strain components in polar coordinates

$\epsilon_{xx}, \epsilon_{yy}$	normal strain components in Cartesian coordinates
σ	uniaxial normal stress, N/m^2
$\sigma_{rr}, \sigma_{\theta\theta}$	normal stress components in polar coordinates, N/m^2
σ_{xx}, σ_{yy}	normal stress components in Cartesian coordinates, N/m^2
σ_y	proportional limit, N/m^2
$\tau_{r\theta}$	shear stress component in polar coordinates, N/m^2
μ	Poisson's ratio

Subscripts:

int	interference
res	residual
max	maximum

FINITE-ELEMENT PROCEDURE

Figure 1 shows the problem analyzed in this study: an aluminum sheet under uniaxial stress with a steel bolt. A value of 10 for w/2R approximated infinite sheet behavior, and a disk, equal in thickness to that of the sheet, represented the bolt.

The finite-element program, described in reference 4, was used to analyze the problem. This program was formulated for plane-stress elements which may be either the conventional uniform-stress type or the more accurate linearly-varying-strain type; furthermore, either type may represent orthotropic or isotropic materials. The program detects the onset of plasticity by the von Mises yield criterion and calculates subsequent plastic response by an incremental loading approach. This program was evaluated in reference 6 for uniaxially loaded sheets with stress concentrations. In the present study, it was modified so that bolt insertion and sheet loading could be analyzed sequentially.

The finite-element model for the sheet is shown in figure 2(a). One quadrant of the sheet and fastener is adequate because of symmetry; the nodes along the X and Y axes were constrained against y and x displacements, respectively. The model has small

linearly-varying-strain elements near the bolt hole because high strain gradients were expected in this region and larger, uniform-strain elements for the remainder of the sheet.

The finite-element model for the bolt is shown in figure 2(b). The bolt and sheet models were connected at nodes along their interface. The bolt-to-sheet interference was produced by expanding the small hole at the bolt center; the bolt stiffness was assumed to be unaffected by this hole.

Both no-slip and no-friction interface conditions were studied. The no-slip condition was assured by joining the bolt and sheet elements at nodes along the interface. The no-friction condition, when interface shear stresses are absent, was assured by giving only radial stiffness to the outer layer of bolt elements. These orthotropic elements are indicated by the shading in figure 2(b).

As previously mentioned, the assumed material properties represented a 7075-T6 aluminum-alloy sheet and a steel bolt. The stress-strain curve for 7075-T6, shown in figure 3, was approximated by a Ramberg-Osgood equation (ref. 7). The bolt had an elastic modulus of 207 000 MN/m^2 and a yield strength high enough to preclude yielding; Poisson's ratio was 0.3 for both materials.

RESULTS AND DISCUSSION

Stress and strain distributions along the X-axis and along the hole boundary are presented for the following cases: a loaded sheet with a clearance-fit bolt (an open hole), an unloaded sheet with an interference-fit bolt, and a loaded sheet with an interference-fit bolt for the two ideal interface conditions, no-slip and no-friction. To enable the results to be compared, a single combination of bolt diameter (6 mm), interference (0.10 mm) and maximum applied stress (300 MN/m^2) was used for all cases. The 0.10 mm interference is a typical value for a 6-mm-diameter bolt (ref. 8). The 300 MN/m^2 maximum applied stress level was chosen to preclude bolt-sheet separation for the cases analyzed. The implications of bolt-sheet separation and fatigue crack initiation are discussed, and although the strain distributions are also presented, they are not discussed.

Clearance-Fit Bolt in a Loaded Sheet

The clearance-fit (open-hole) case provided a reference against which the two interference-fit cases were evaluated; stress and strain distributions for the clearance-fit case are presented in figure 4. The stress distributions on the X-axis and the corresponding strain distributions are shown in figure 4(a) and 4(b), respectively. The distributions are shown as solid curves for $S_{max} = 300\ MN/m^2$ and as dash-dot curves for the residual state after unloading to $S = 0$. These two conditions are indicated by the subscripts max and res, respectively.

The largest value of σ_{yy} in figure 4(a) does not occur at $\frac{x}{R} = 1$, as in the elastic case, but instead at a point where $\frac{x}{R} > 1$. The tensile σ_{xx} for values of $\frac{x}{R} > 1$ influenced yielding and caused this shift. (Note that the yield zone extends to $\frac{x}{R} = 1.4$.) According to the von Mises yield criterion (for $y = 0$)

$$\sigma_y = \left(\sigma_{xx}^2 + \sigma_{yy}^2 - \sigma_{xx}\sigma_{yy}\right)^{1/2} \tag{1}$$

higher values of σ_{yy} occur for $\frac{x}{R} > 1$ where $\sigma_{xx} > 0$ rather than at the hole boundary where $\sigma_{xx} = 0$.

During unloading from 300 MN/m^2 the local stresses decreased elastically. Consequently, for subsequent cyclic loading from 0 to 300 MN/m^2, the local stresses will cycle elastically between the values indicated by the dash-dot and solid curves. At the hole boundary, σ_{yy} will cycle from -320 to 560 MN/m^2; this range corresponds to a stress concentration factor of 2.93 based on gross-section nominal stress. This value agrees well with the theoretical value of 3 for a hole in an infinite plate.

The stress and strain distributions along the hole boundary are presented in figures 4(c) and 4(d). As expected, the largest range of $\sigma_{\theta\theta}$ occurred at the X-axis ($\theta = 0$). Yielding extended from the X-axis to $\theta = 30^\circ$.

Interference-Fit Bolt in an Unloaded Sheet

Figure 5 shows stress and strain distributions produced by inserting a steel interference-fit bolt into a 7075-T6 sheet. These distributions are not influenced by slip or friction at the bolt-sheet interface because interference produces only radial forces at the interface.

The solid curves in figure 5(a) show stress distributions for a 0.038 mm interference or the level for incipient yielding at the hole. Because of the biaxial stress state ($\sigma_{xx} = -\sigma_{yy}$), yielding at the hole occurs for a stress magnitude of 279 MN/m^2, which is only about 60 percent of the uniaxial yield stress. The 0.038 mm interference level is smaller than the minimum level recommended in reference 9 by an interference-fit bolt manufacturer and thus recommended interference levels will cause the sheet to yield.

Results for 0.05 mm and 0.10 mm interference levels are shown in figure 5 as dash-dot and dashed curves, respectively. Because of yielding, the maximum values of σ_{yy} occur near the boundary of the yield zones, not at the edge of the hole. Outside the yield zones, the curves resemble those for the elastic case.

Interference-Fit Bolt in a Loaded Sheet

No-slip interference.- Results for the no-slip case are presented in figure 6. The stress and strain distributions are shown as dashed curves for bolt insertion, as solid curves for the maximum load, and as dash-dot curves for the residual state after unloading. These three conditions are indicated by the subscripts int, max, and res, respectively.

Figure 6(a) shows that the 300 MN/m^2 applied stress extended the yield zone from $\frac{x}{R} = 1.6$ to $\frac{x}{R} = 2.5$. This additional yielding altered the stresses caused by the interference fit. (Compare the dashed curves with the dash-dot curves.)

As in the clearance-fit case, the sheet unloaded elastically when the 300 MN/m^2 stress was removed. Consequently, for subsequent 0 to 300 MN/m^2 cyclic loading, the local stresses will cycle elastically between the values shown by the dash-dot and solid curves. At the hole, σ_{yy} will cycle between 90 and 230 MN/m^2. This range corresponds to a stress concentration factor of 0.47, which agrees with the theoretical elastic value of 0.45 from reference 1. Thus, yielding produced by bolt insertion and by the applied load altered only the local mean stress, not the local stress range. In contrast to the clearance-fit case, both the mean and range for σ_{yy} are larger away from the hole than at the hole.

The stresses along the hole boundary are presented in figure 6(c). The dash-dot and solid curves show that the $\sigma_{\theta\theta}$ range is largest at $\theta = 0$; whereas, the σ_{rr} and $\tau_{r\theta}$ ranges are largest elsewhere. The σ_{rr} range (largest at $\theta = 90^o$) should not influence fatigue life because σ_{rr} is compressive. But the $\tau_{r\theta}$ range, which represents cyclic shear stress on the interface, will probably result in slip for real interface conditions and therefore cause fretting. Slip and hence fretting are most likely to occur between $\theta = 40^o$ and $\theta = 60^o$ where the maximum range of $\tau_{r\theta}$ occurs.

Figure 6(c) illustrates why the stress range near a hole with an interference bolt is smaller than that for an open hole. The stress components σ_{rr} and $\tau_{r\theta}$ shown here act on the interface and thus they indicate the amount of load transferred between the bolt and sheet. The large difference between the $(\sigma_{rr})_{max}$ and the $(\sigma_{rr})_{res}$ curves near $\theta = 90^o$ shows that a portion of the applied tensile load transfers across the bolt hole by reducing the compressive stresses acting on the bolt. The difference between the $(\tau_{r\theta})_{max}$ and $(\tau_{r\theta})_{res}$ curves near $\theta = 50^o$ shows that load also transfers across the bolt hole by shear loading on the bolt. Because some of the applied load transfers across a hole with an interference-fit bolt, the hole deflects less load than one with a clearance-fit bolt. Consequently, the hole with the interference-fit bolt causes a smaller stress concentration and, therefore, the local stress range for the interference-fit case is smaller than that for the clearance-fit case.

No-friction interference.- Stress and strain distributions for a uniaxially loaded sheet with a no-friction interference bolt are presented in figure 7. For this case, less load

passes through the bolt because shear stresses do not develop at the interface. Accordingly, the local stress ranges in the sheet are larger than those for the no-slip case. At the hole, σ_{yy} cycles between -130 and 260 MN/m^2 for a stress concentration factor of 1.30, as compared with 0.47 for the no-slip case. The 1.30 stress concentration factor agrees with the 1.33 theoretical elastic value from reference 1; this agreement indicates that the orthotropic finite elements at the interface adequately modeled the no-friction case.

Figure 7(c) shows that $(\sigma_{r1})_{max}$ equals zero at $\theta = 90^o$ for $S_{max} = 300$ MN/m^2. Therefore, for an applied stress larger than 300 MN/m^2, the sheet will separate from the bolt. Because the present analysis did not account for separation, 300 MN/m^2 was the largest applied stress considered.

Separation at the bolt-sheet interface.- The minimum applied stresses required for separation at $\theta = 90^o$ are shown in figure 8 for various interference levels. The no-slip and no-friction curves bracket the onset of separation for all possible interface conditions because they represent extreme conditions, as previously mentioned. Separation will not occur below the no-friction curve and must occur above the no-slip curve.

For loading after separation occurs, less load passes through the bolt; therefore, the bolt has less effect on fatigue life. The recommended interference range (ref. 9) for a 6 mm bolt is shown in figure 8. Separation stresses for the upper limit of the range are about 50 percent larger than those for the lower limit. Separation may be responsible for the shorter fatigue lives generally observed for the lower interference levels (for example, see ref. 8).

The separation curves in figure 8 were calculated for tensile loading only and are not expected to apply for cases involving compressive loads. Because the sheet yields when the bolt is inserted, even small compressive loads will cause additional compressive yielding near $\theta = 90^o$ and will reduce the residual contact stresses. Consequently, for subsequent tensile loading, the sheet will separate from the bolt at lower loads than those indicated in figure 8, and thus compressive loads are expected to reduce the effectiveness of interference bolts during subsequent tensile loading.

Fatigue Analysis

Crack initiation periods for the two interference cases were estimated by using fatigue data from reference 10 for unnotched specimens and calculated local stresses. For comparison, the crack initiation period was also estimated for the clearance-fit case. All estimates were for 0 to 300 MN/m^2 cyclic loading.

Conventional methods for biaxial fatigue analysis, based on alternating shear stress, could not be used in the present study because the principal shear planes rotated during the load cycle. Furthermore, the alternating normal stresses on the principal shear planes

were out of phase with the alternating shear stress. For simplicity and because these cyclic stress state effects and possible fretting effects could not be analyzed, fatigue crack initiation was assumed to be governed by maximum alternating normal stress.

Crack initiation periods were estimated by the following procedure. First, the maximum and residual stresses were calculated for a network of points near the hole. Then, the alternating and mean normal stresses in the direction of the largest alternating normal stress were calculated. Next, these alternating and mean stresses were compared with unnotched specimen data to estimate a crack initiation period for each point. The crack initiation period for the sheet was taken as the shortest for the network; accordingly, the crack was assumed to initiate at the point with the shortest period.

For each interference-fit case, the point with the shortest crack initiation period was at $\frac{x}{R} = 2$ on the X-axis. The crack initiation periods are presented in figure 9 and are compared with those for the clearance-fit case and for an unnotched specimen. The unnotched specimen life is presented because the sheet would behave as an unnotched specimen if the interference-fit bolt eliminated the detrimental effect of the hole. Therefore, the unnotched specimen life is an upper limit for the interference-fit cases.

The crack initiation periods were estimated to be about 100 000 cycles for the unnotched specimen and 1000 cycles for the clearance-fit case (open hole). The hole reduced the crack initiation period to 1 percent of that for the unnotched specimen. Crack initiation periods for the no-slip and no-friction cases were estimated to be 60 000 and 50 000 cycles, respectively, which are 60 and 50 percent of the values for the unnotched specimen. The estimated crack initiation periods were similar because the cyclic stresses were similar at the crack initiation site for the two cases. (Compare stresses at $\frac{x}{R} = 2$ in figs. 6(a) and 7(a).)

Reference 10 contains the observed fatigue lives of 700 and 35 000 cycles for 7075-T6 specimens with open countersunk holes (clearance-fit case) and with countersunk holes containing steel interference-fit bolts, respectively. These lives compare reasonably well with the estimated 1000 cycles for the clearance-fit case and with the 50 000 and 60 000 cycles for the interference-fit cases. The countersunk configuration used in reference 10 is probably responsible for the discrepancies between the observed and estimated lives. An open countersunk hole causes a stress concentration which is larger than that for the open hole analyzed in the present study, and a countersunk hole with an interference bolt has very little interference over the countersunk portion of the hole. Both of these effects could cause the observed lives to be shorter than estimated.

Reference 10 reports that for the interference-fit bolt, the cracks initiated at $3 \leq \frac{x}{R} \leq 5$ rather than at $\frac{x}{R} = 2$ as estimated in the present study. This discrepancy may be caused by the difference in sheet widths; in the present study the ratio of sheet width to bolt diameter was 10, but it was only 5.3 in reference 10.

CONCLUDING REMARKS

Elastoplastic stresses and strains for a loaded sheet with an unloaded interference-fit bolt have been calculated by a finite-element analysis. Material characteristics represented a 7075-T6 aluminum-alloy sheet and a steel bolt. The two ideal cases examined, no slip at the interface between the bolt and sheet and no friction at the interface, bracket the real interface behavior which is expected to involve both slip and friction. The analysis was limited to a load range for which the bolt and sheet remained in contact.

Bolts, when inserted with recommended interference levels, were shown to plastically deform the sheet near the bolt hole. The first tensile load cycle produced additional yielding, but subsequent cycles caused only elastic local stress excursions.

The remote uniaxial load required to separate the sheet from the bolt was shown to be about 50 percent higher at the upper limit of a bolt manufacturer's recommended interference range than it was at the lower limit of interference. Bolt-sheet separation may be responsible for the shorter fatigue lives generally observed for the smaller interference levels.

Fatigue life estimates based on the calculated local stresses showed, for the case examined, that if a clearance-fit bolt was replaced by an interference-fit bolt, the crack initiation period was about 50 times longer. Crack initiation was predicted to occur on the transverse axis at a distance of one radius from the hole for both the no-slip and no-friction cases. At this location, the cyclic stresses for the two cases were nearly equal; therefore, the predicted crack initiation periods were also nearly equal. The estimated crack initiation periods and the initiation site agreed with test results from the literature.

Langley Research Center,
National Aeronautics and Space Administration,
Hampton, Va., August 26, 1974.

REFERENCES

1. Crews, John H., Jr.: An Elastic Analysis of Stresses in a Uniaxially Loaded Sheet Containing an Interference-Fit Bolt. NASA TN D-6955, 1972.

2. Brombolich, Lawrence J.: Elastic-Plastic Analysis of Stresses [illegible] Fas[illegible] Holes. AIAA Paper No. 73-252, Jan. 1973.

3. Allen, Merle; and Ellis, J. A.: Stress and Strain Distribution in the Vicinity of Interference Fit Fasteners. AFFDL-TR-72-153, U.S. Air Force, Jan. 1973.

4. Isakson, G.; Armen, H., Jr.; and Pifko, A.: Discrete-Element Methods for the Plastic Analysis of Structures. NASA CR-803, 1967.

5. Mechtly, E. A.: The International System of Units – Physical Constants and Conversion Factors (Second Revision). NASA SP-7012, 1973.

6. Armen, M., Jr.; Pifko, A.; and Levine, H. S.: Finite Element Analysis of Structures in the Plastic Range. NASA CR-1649, 1971.

7. Ramberg, Walter; and Osgood, William R.: Description of Stress-Strain Curves by Three Parameters. NACA TN 902, 1943.

8. Urzi, Robert B.: Development of Fatigue Test Standards and Mechanical Property Data on Interference Fit Fastener Systems. AFML-TR-73-195, U.S. Air Force, Aug. 1973.

9. Mead, Daniel R.: Taper-Lok Reference Manual. Second ed., Briles Manufacturing, c.1967.

10. Smith, Clarence R.: Interference Fasteners for Fatigue-Life Improvement. Exp. Mech., vol. 5, no. 8, Aug. 1965, pp. 19A-23A.

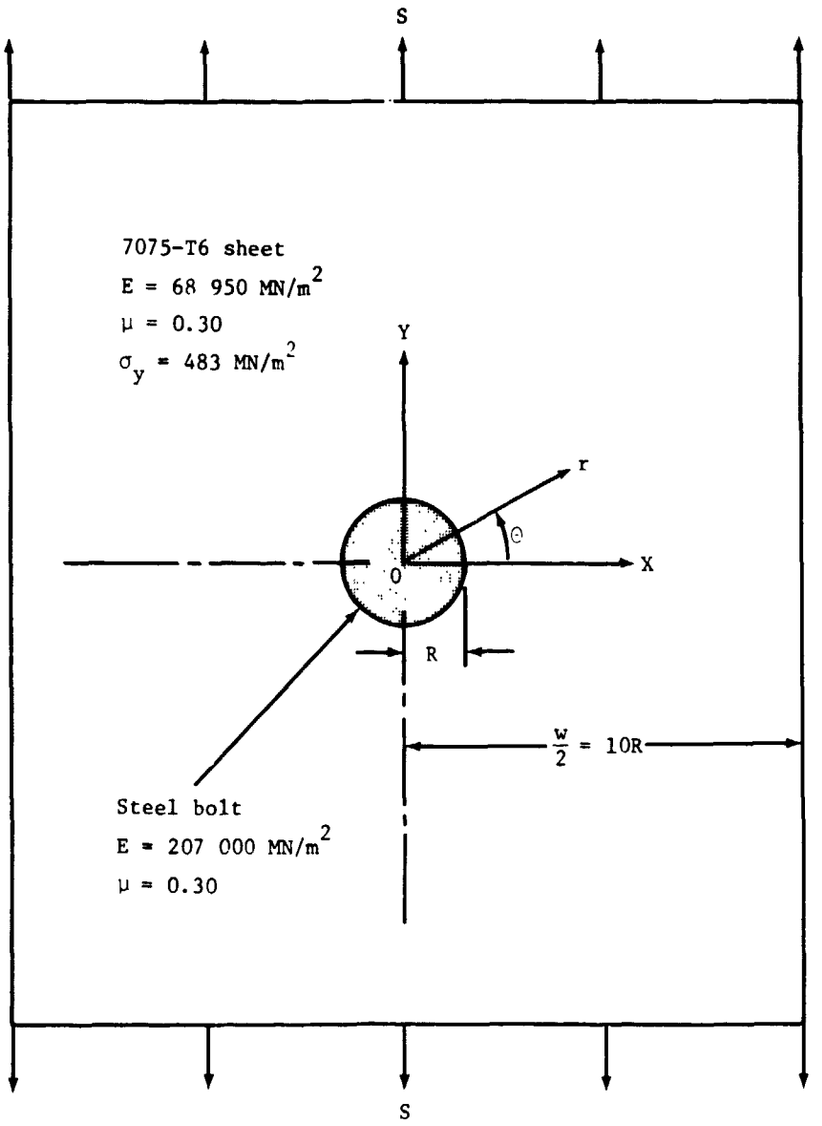

Figure 1.- Sheet under uniaxial stress with an interference-fit disk.

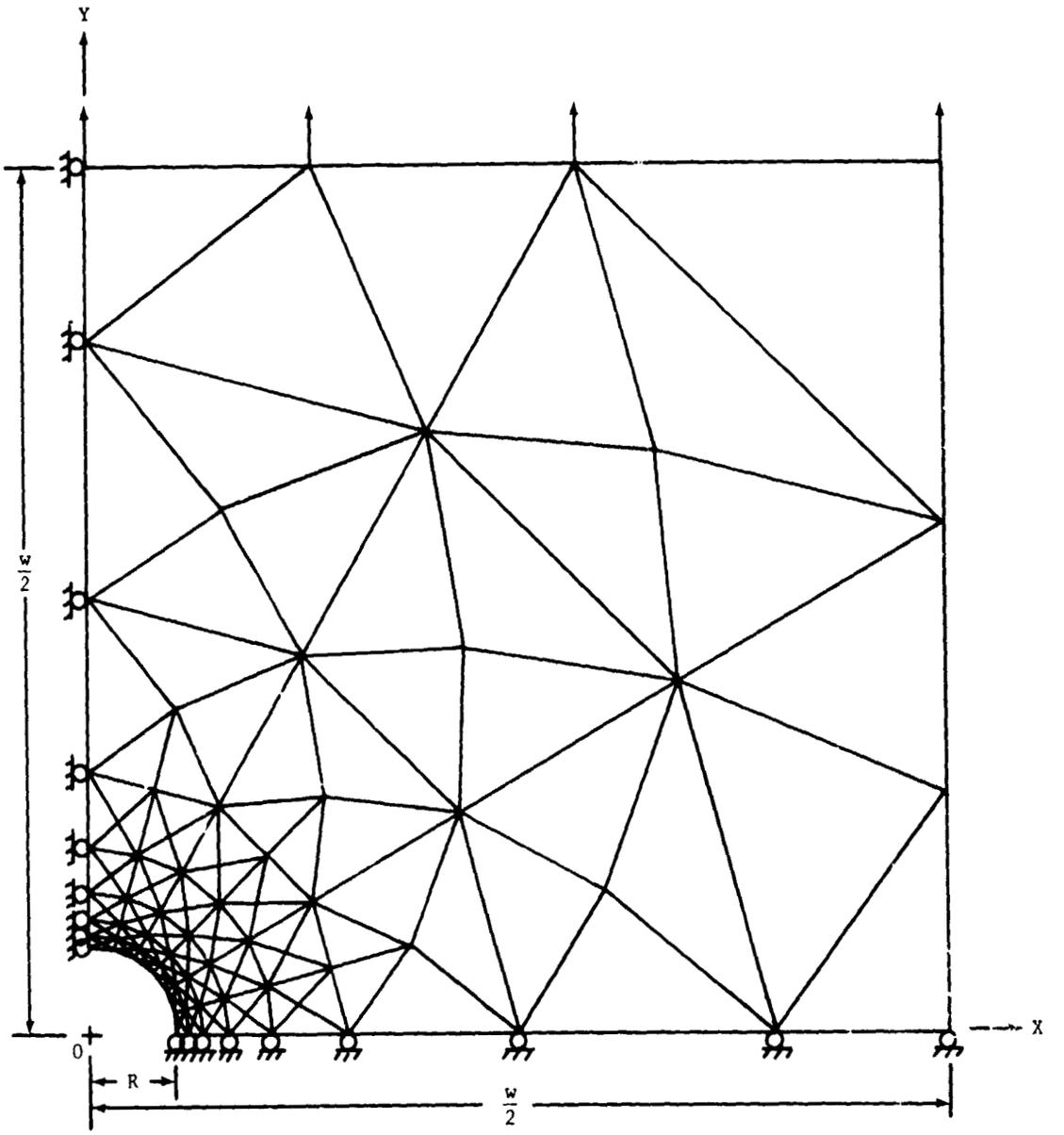

(a) Sheet with a bolt hole.

Figure 2.- Finite-element model.

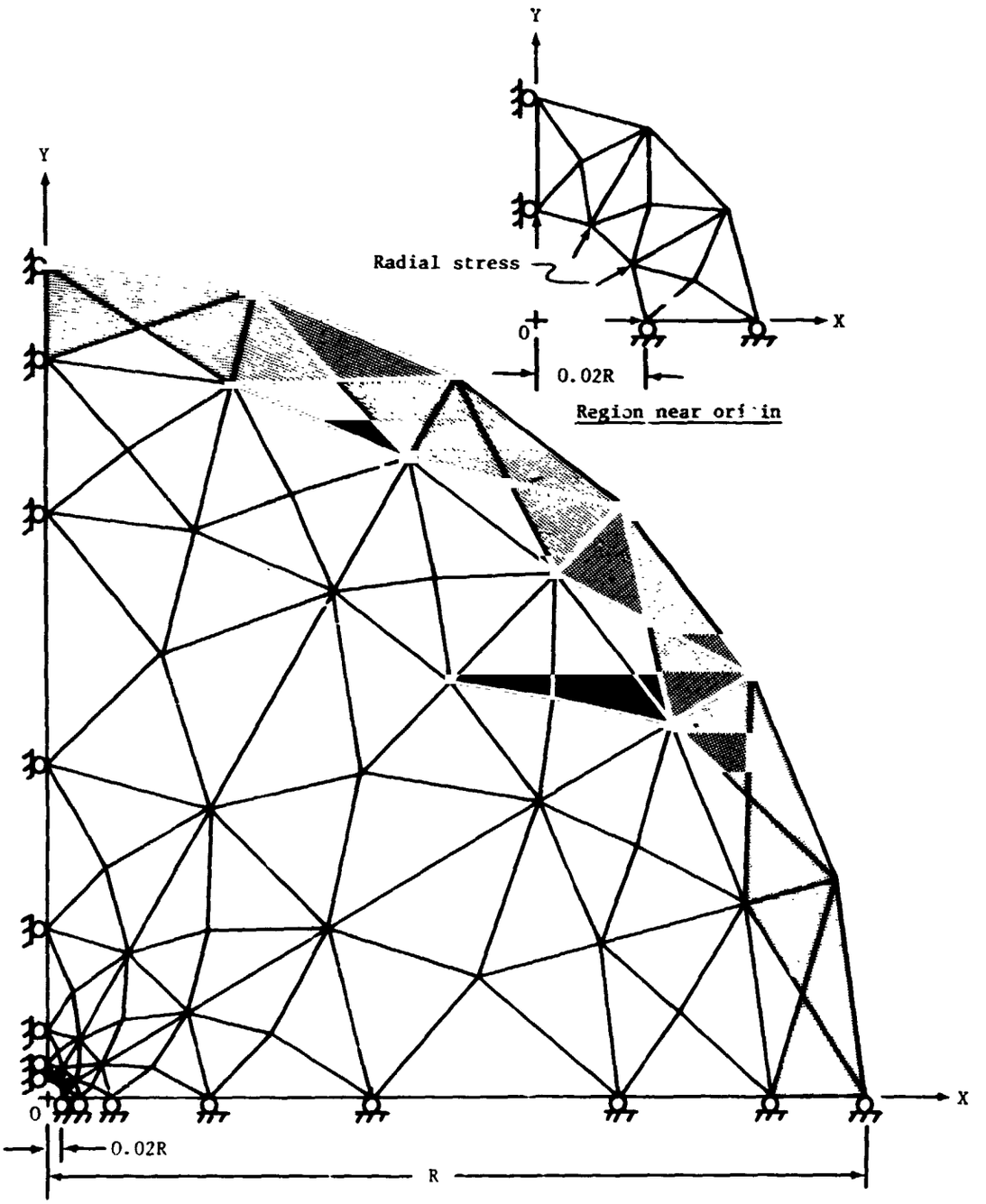

(b) Bolt.

Figure 2.- Concluded.

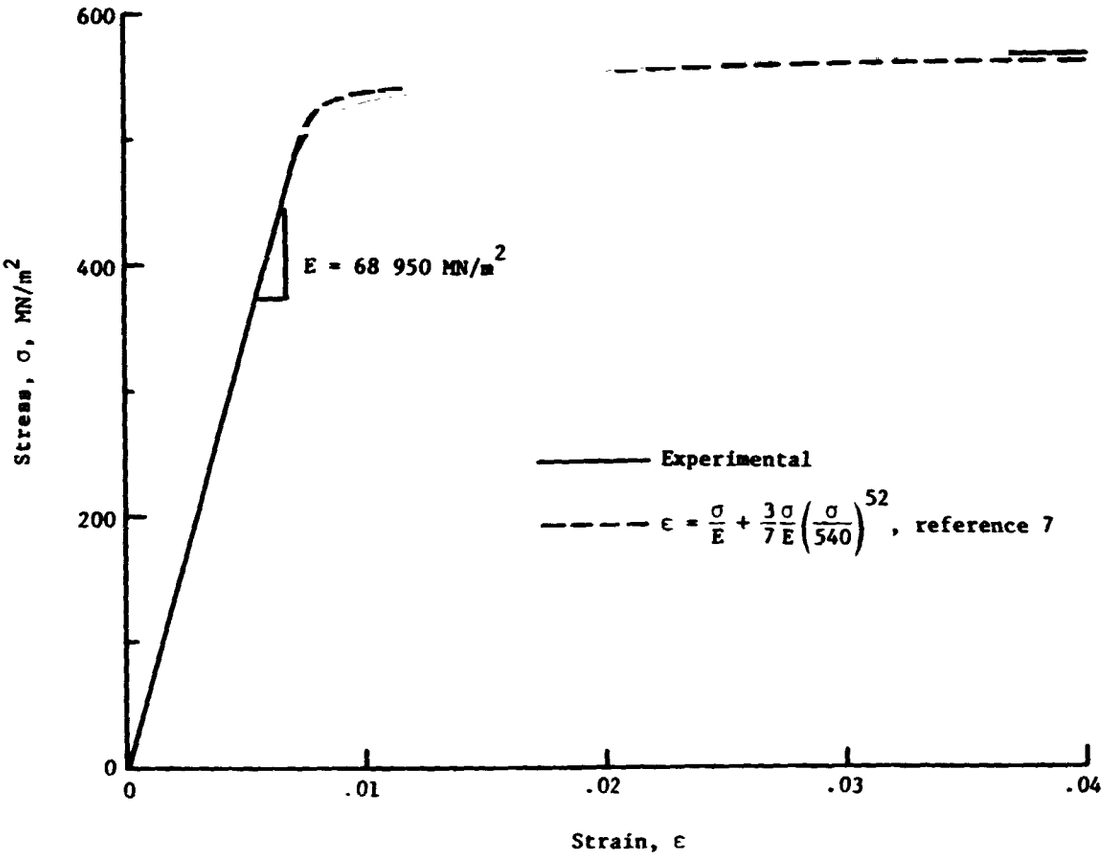

Figure 3.- Stress-strain curves for 7075-T6 aluminum-alloy sheet.

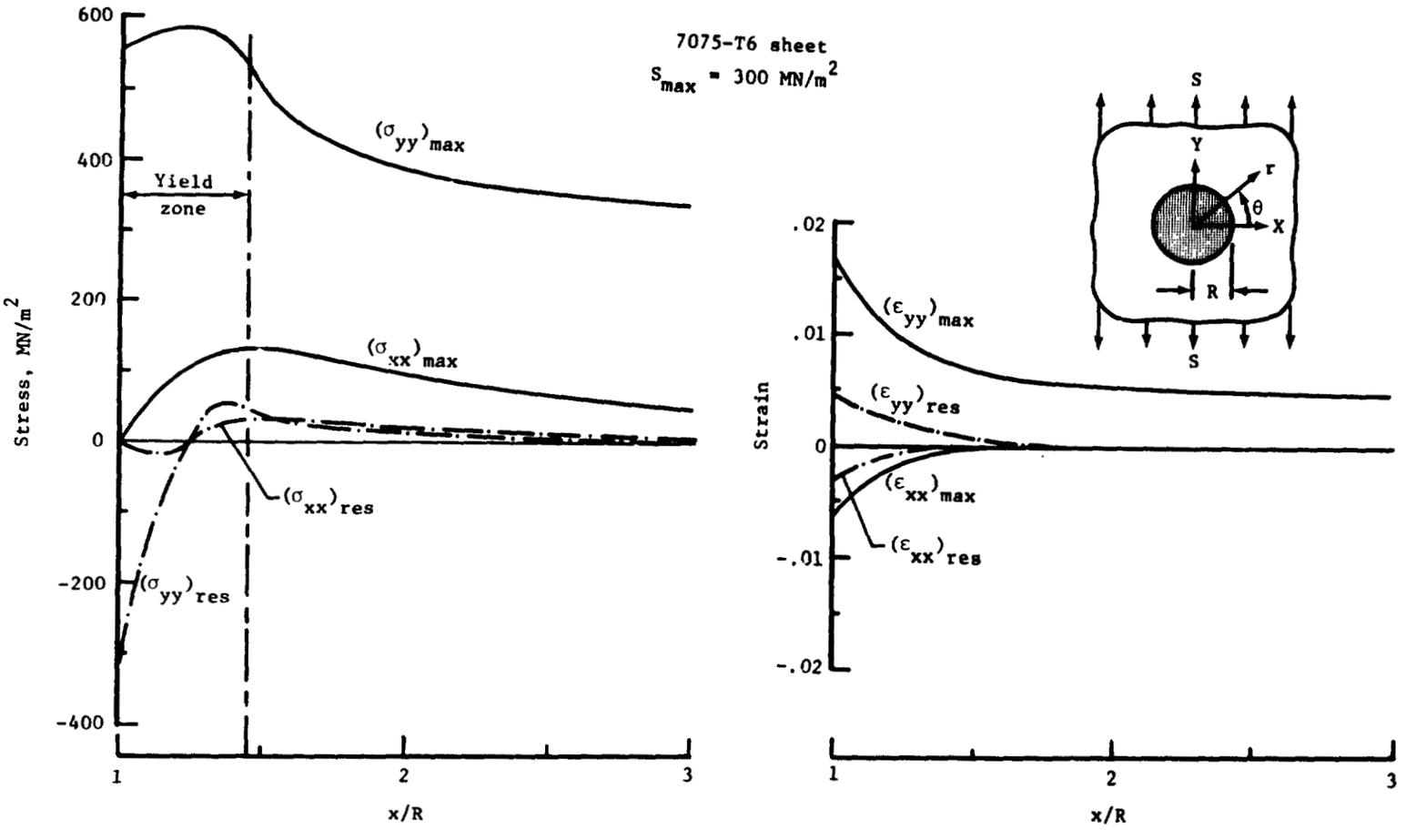

(a) Stress distributions along the X-axis.

(b) Strain distributions along the X-axis.

Figure 4.- Stress and strain distributions for a clearance-fit bolt in a loaded sheet.

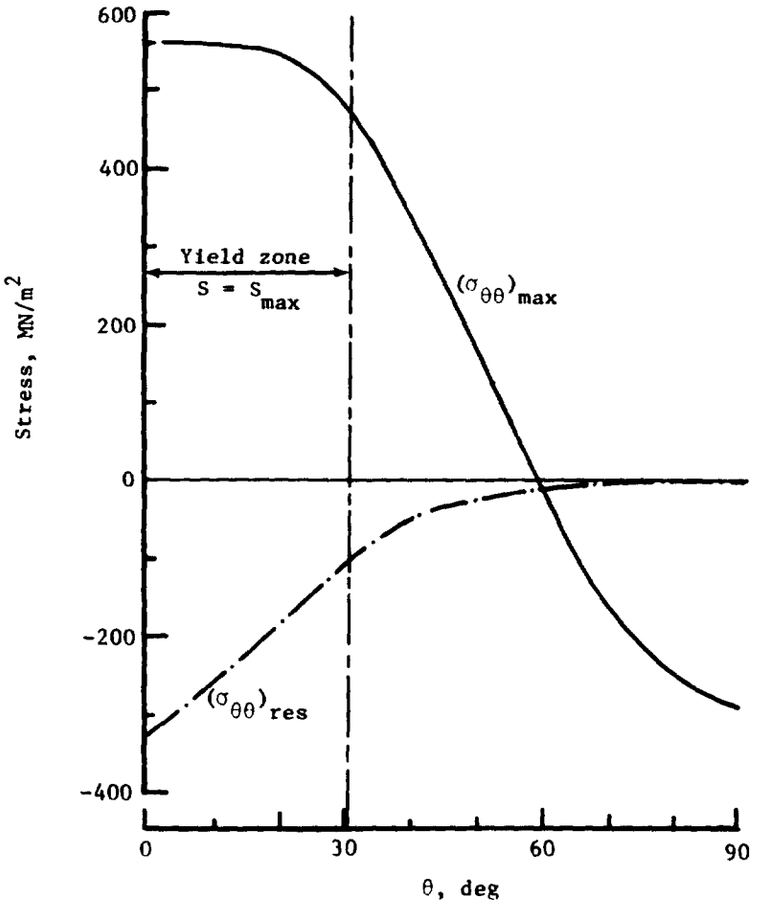

(c) Stress distributions along the hole boundary.

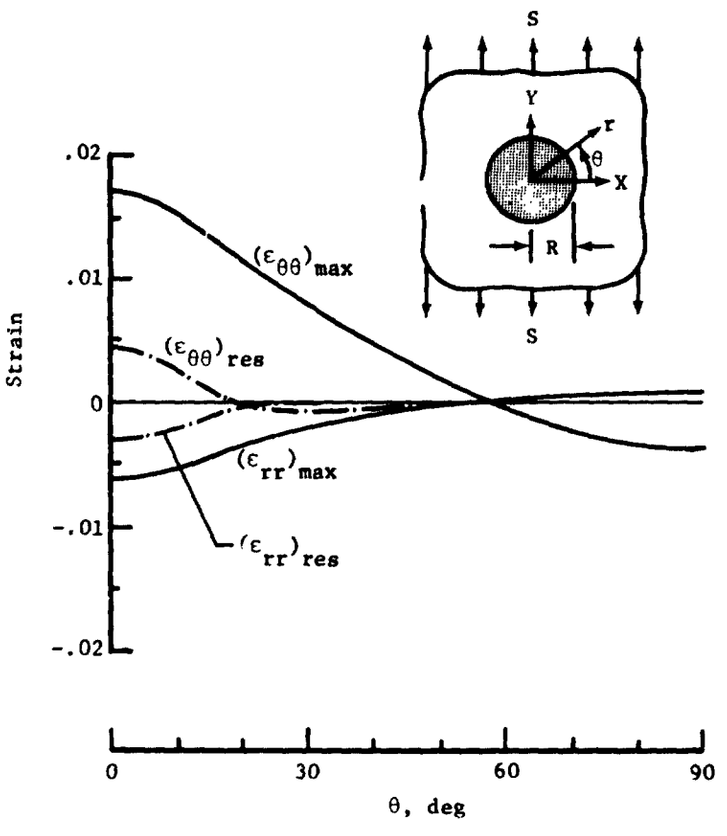

(d) Strain distributions along the hole boundary.

Figure 4.- Concluded.

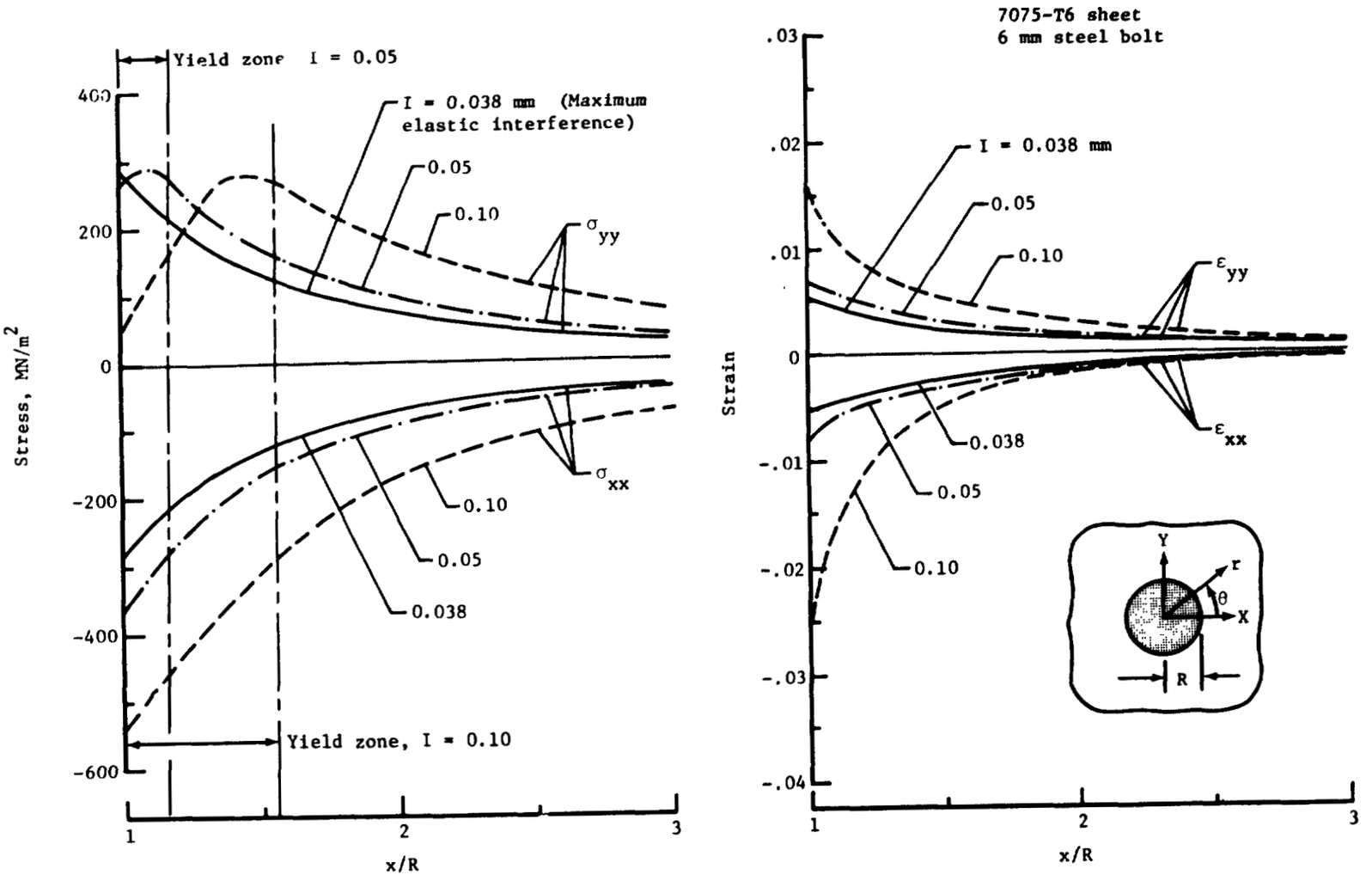

(a) Stress distributions along the X-axis.

(b) Strain distributions along the X-axis.

Figure 5.- Stress and strain distributions for an interference-fit bolt in an unloaded sheet.

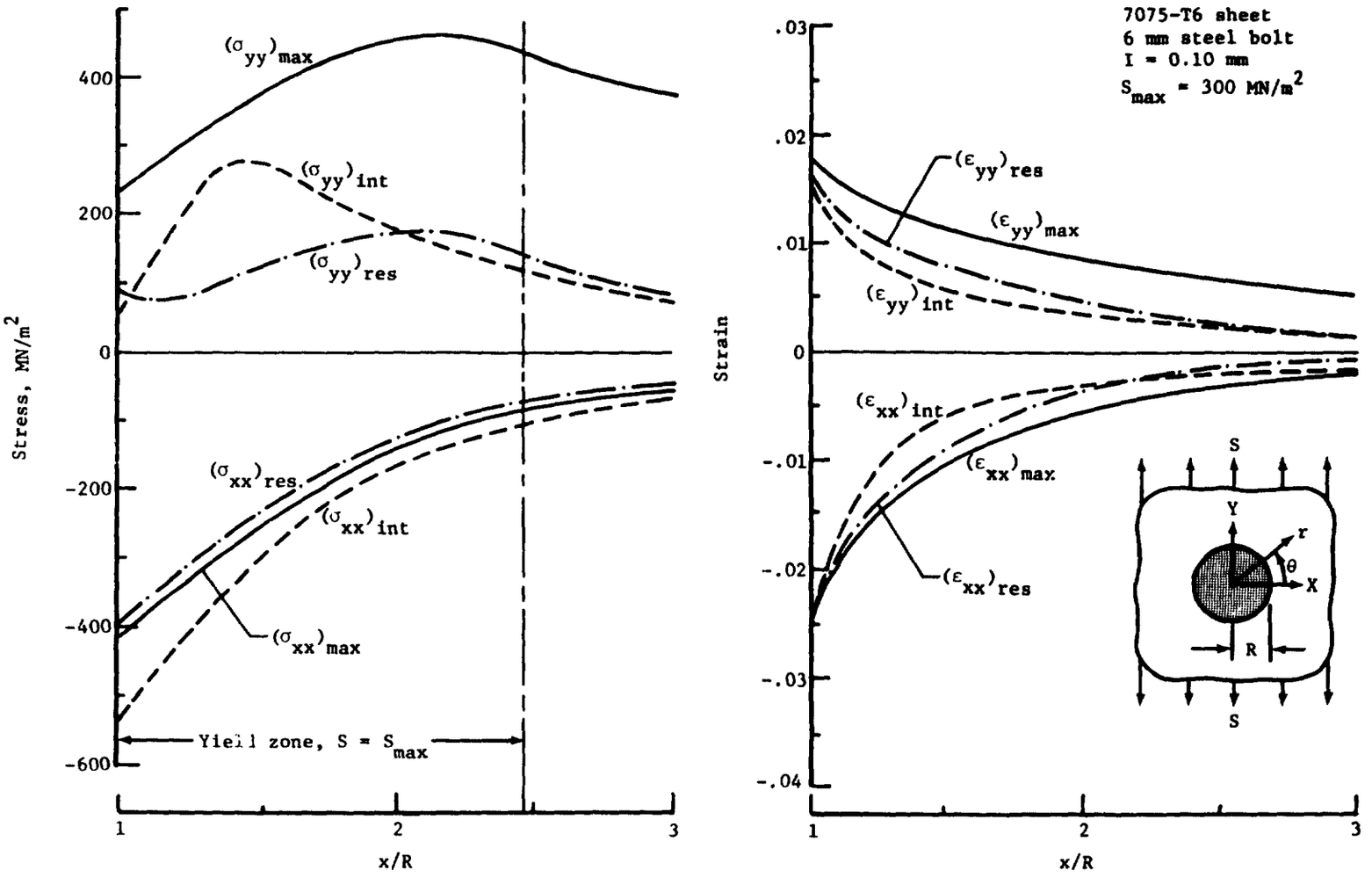

(a) Stress distributions along the X-axis.

(b) Strain distributions along the X-axis.

Figure 6.- Stress and strain distributions for a no-slip interference bolt in a loaded sheet.

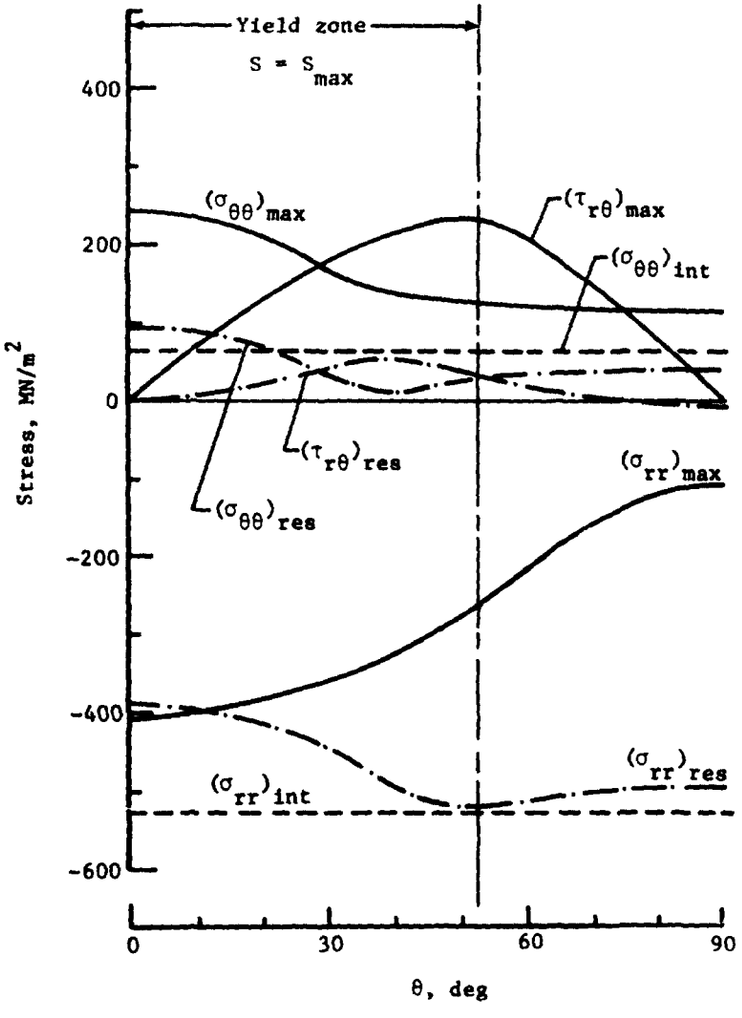

(c) Stress distributions along the hole boundary.

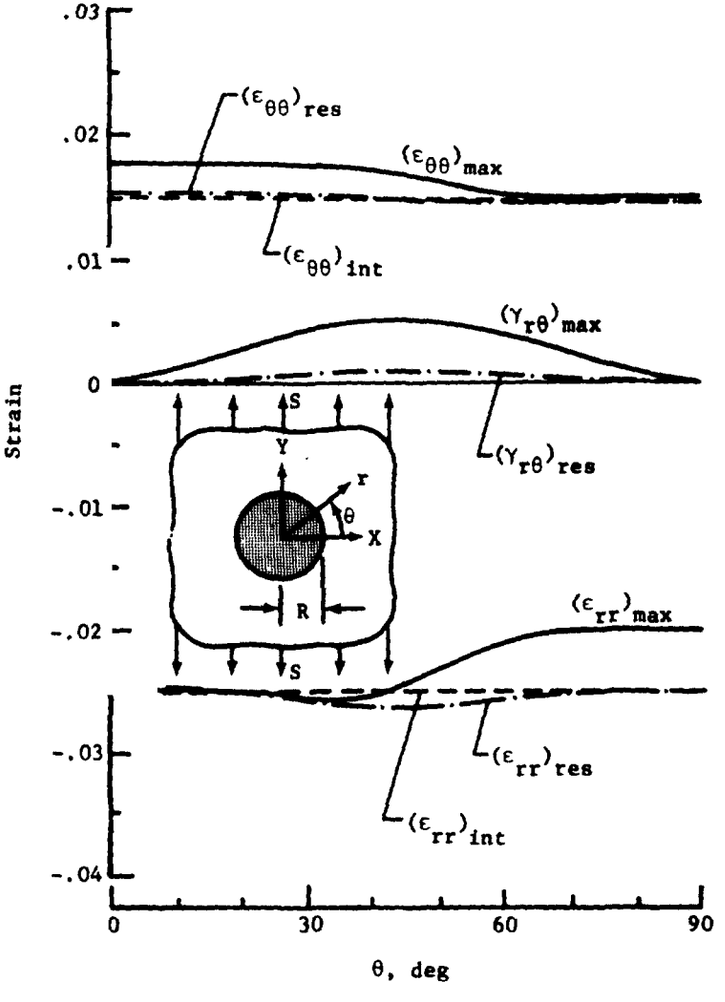

(d) Strain distributions along the hole boundary.

Figure 6.- Concluded.

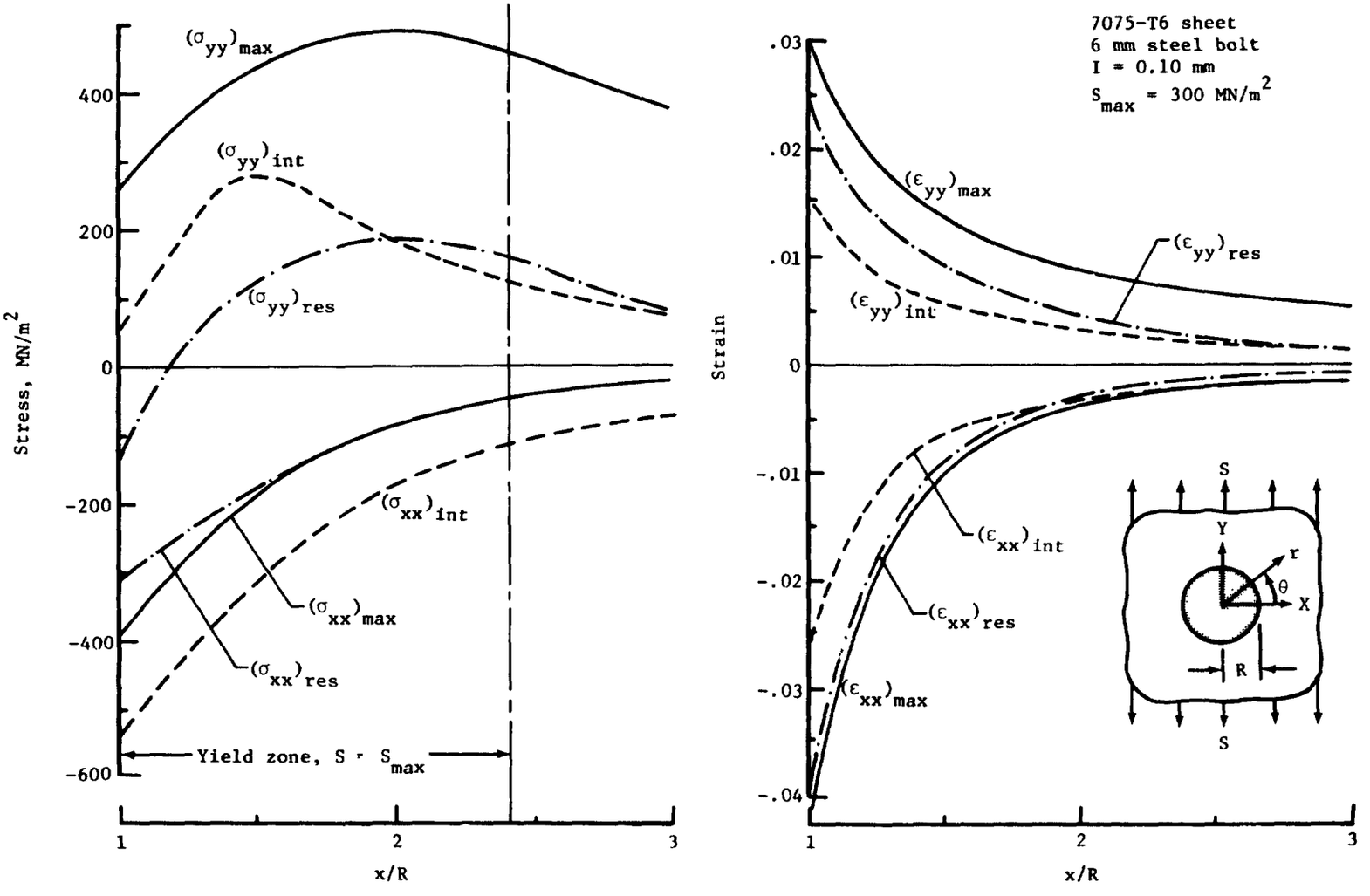

(a) Stress distributions along the X-axis.

(b) Strain distributions along the X-axis.

Figure 7.- Stress and strain distribution for a no-friction interference bolt in a loaded sheet.

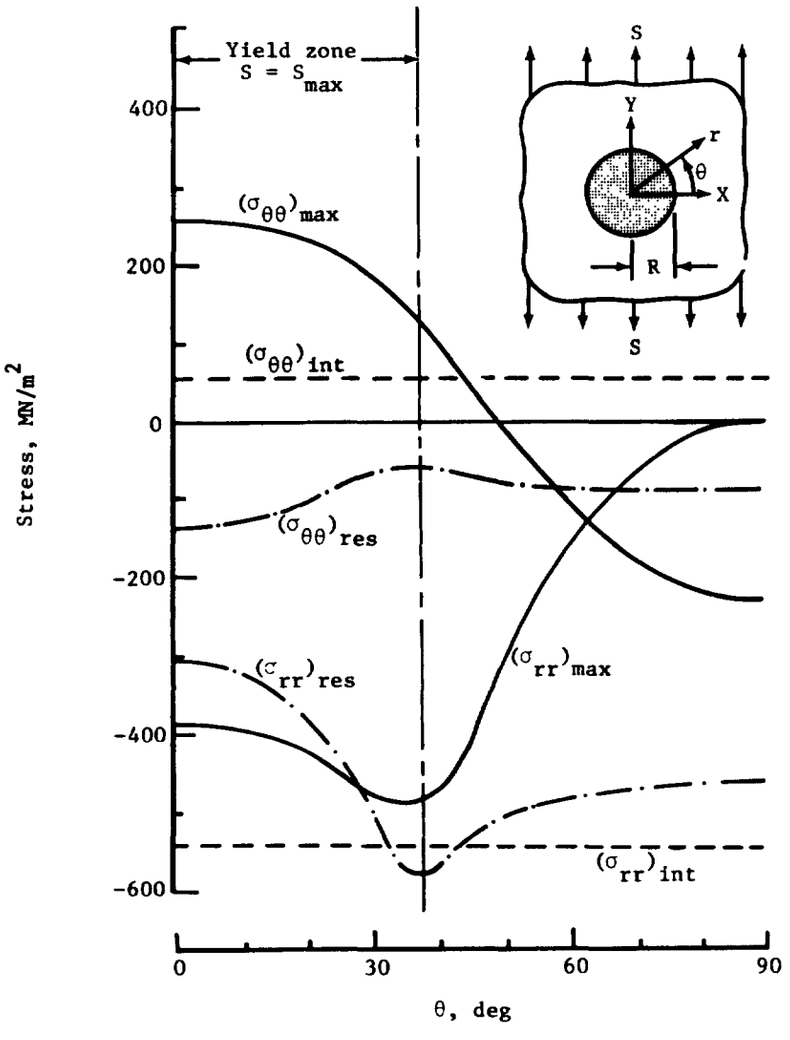

(c) Stress distributions along the hole boundary.

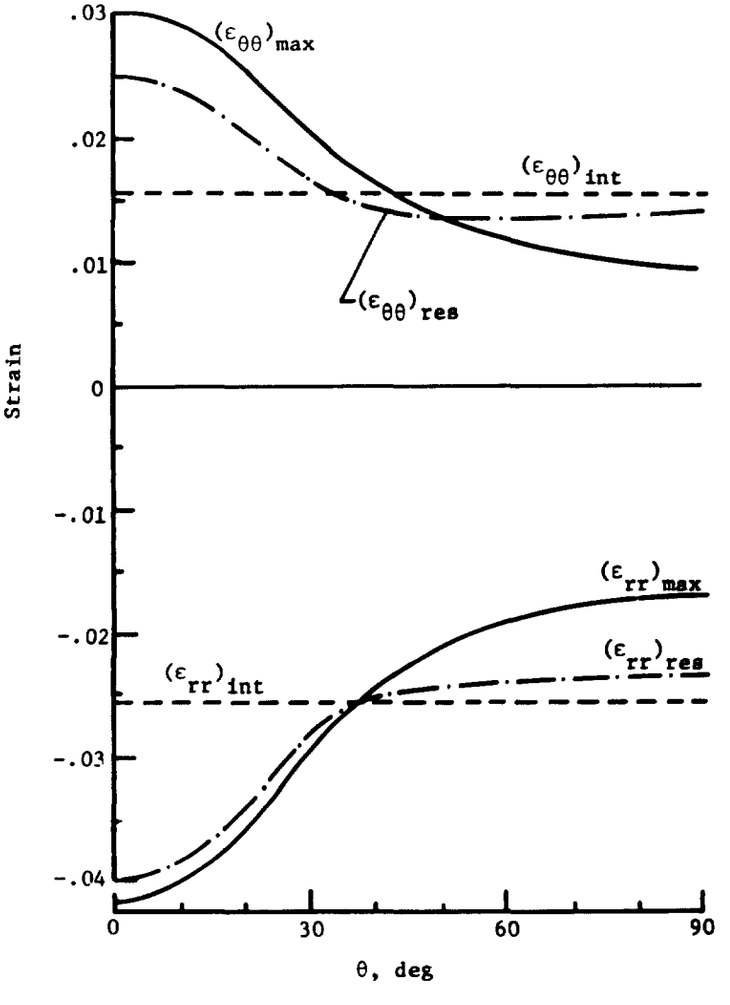

(d) Strain distributions along the hole boundary.

Figure 7.- Concluded.

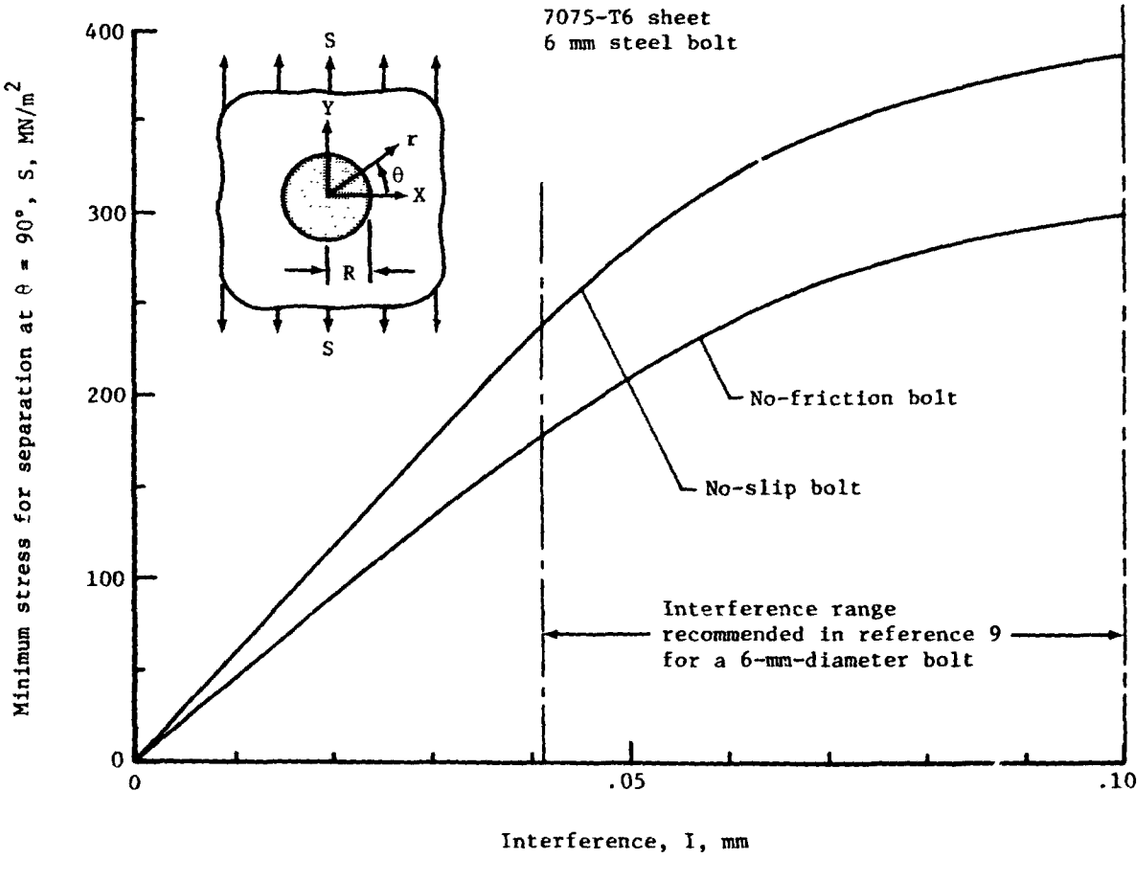

Figure 8.- Applied stress required for separation at the bolt-sheet interface.

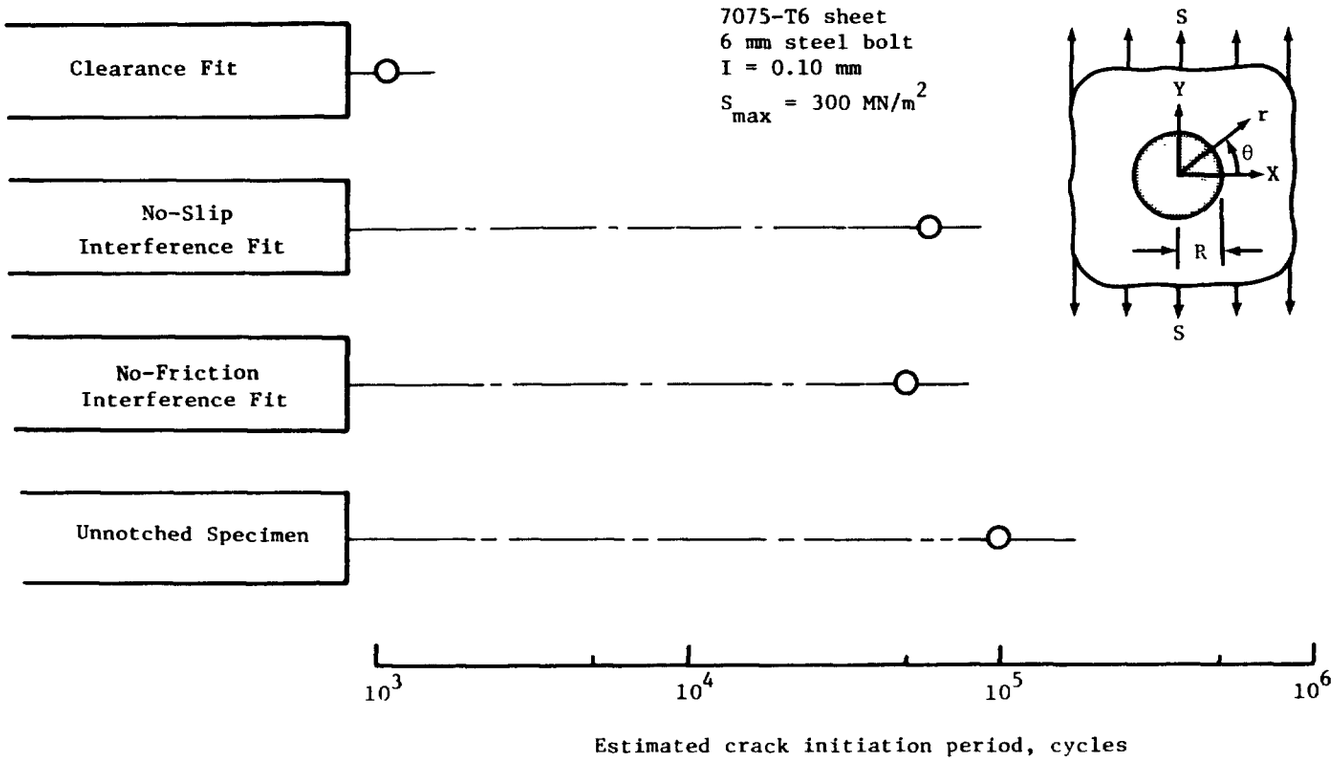

Figure 9.- Fatigue predictions for a uniaxially loaded sheet with an interference-fit fastener.